Kernel-based Meshless Collocation Methods for Solving Coupled Bulk-surface Partial Differential Equations

Meng Chen · Leevan Ling

29th, July, 2019

Abstract A meshless kernel-based method is developed to solve coupled second-order elliptic PDEs in bulk domains and surfaces, subject to Robin boundary conditions. It combines a least-squares kernel collocation method with a surface-type intrinsic approach. Therefore, we can use each pair for discrete point sets, RBF kernels (globally and restrictedly), trial spaces, and some essential assumptions, for the search of least-squares solutions in bulks and on surfaces respectively. We first give error estimates for domain-type Robin-boundary problems. Based on this and existing results for surface PDEs, we discuss the theoretical requirements for the employed Sobolev kernels. Then, we select the orders of smoothness for the kernels in bulks and on surfaces. Lastly, several numerical experiments are demonstrated to test the robustness of the coupled method for accuracy and convergence rates under different settings.

Keywords Meshless collocation methods · Coupled bulk-surface PDEs · Smoothness orders of global and restricted kernels · Error estimate

Mathematics Subject Classification (2010) 65D15 · 65N35 · 41A63

This work was supported by a Hong Kong Research Grant Council GRF Grant and a Hong Kong Baptist University FRG Grant.

M. Chen
Hong Kong Applied Science and Technology Research Institute Company Limited, Shatin, Hong Kong
E-mail: chenmeng@astri.org

L. Ling
Department of Mathematics, Hong Kong Baptist University, Kowloon Tong, Hong Kong
E-mail: lling@hkbu.edu.hk

1 Introduction

In recent years, coupled surfaces (or interfaces) and bulk partial differential equation (PDE) models have been widely used in many applications. Examples include characterization of electrospun membranes [17], proton diffusion along biological membranes [15], bulk mediated surface diffusion [3], and a topological insulator [9] in material science. Most of these can be reduced to a basic problem coupling bulk and surface elliptic PDEs, subject to Robin-type boundary conditions.

In [7], a finite element method (FEM) using two trial spaces was proposed: a polyhedral approximation was employed in the the bulk domain, whereas piecewise polynomial boundary faces were used on the surface. A cut finite element method that uses continuous piecewise linear elements defined in both the bulk domain and the surface can be found in [2]. In [1], one can find a diffuse domain method for solving coupled bulk-surface PDEs. The method extends the systems into a larger domain, subject to additional terms to approximate the original boundary, in order to yield numerical solutions.

In this work, we propose a bulk-surface meshless collocation method by combining the domain and surface-type approaches respectively in [4,6]. The latter method is intrinsic to surface without extension to narrow domains for embedded PDEs used in [5,11–13,18,19]. The coupled systems introduced in Section 2. Section 3 presents two types of preliminary settings for discretization and error measurement in terms of the bulk PDE and surface PDE respectively. In Section 4, we provide convergence property of weighted least-squares solutions for solving general second-order elliptic bulk problems with Robin boundary conditions. Section 5 gives the implementation details of the proposed method with oversampling for a system of bulk-surface equations. Besides, we discuss error estimates under some theoretical requirements of kernels for the coupled PDEs. In Sections 6, we run several numerical experiments to test our methods by utilizing oversampling conditions, various smoothness orders of kernels and discretized settings for bulks and surfaces. Lastly, we demonstrate simulations by imposing different source terms.

2 Coupled bulk-surface elliptic PDEs

Initially, we require smoothness assumptions in the problem domain and its boundary for error estimates being discussed in Sections 4 and 5, as below.

Assumption 1 *(Smoothness of domain and boundary). We assume that the bounded smooth domain Ω in $\mathbb{R}^d$ has a closed, connected and complete boundary $\mathcal{S}$ of dimensions $d_{\mathcal{S}} = d - 1$. Let Ω be Lipschitz continuous and satisfy an interior cone condition [6, Assumption 2.1], and $\mathcal{S}$ is of class $\mathcal{C}^{\mu+1}$ for some integer μ with bounded geometry and satisfies a boundary regularity in [4, Assumption 1].*

A second-order elliptic PDE coupled in the bounded domain Ω and on the surface $\mathcal{S}$ is in the form of

$$-\Delta u_B + u_B = f_B, \quad \text{in } \Omega, \tag{1}$$
$$(\alpha u_B - \beta u_{\mathcal{S}}) + \partial_{\boldsymbol{n}} u_B = g_{\mathcal{S}}, \quad \text{on } \mathcal{S}, \tag{2}$$
$$-\Delta_{\mathcal{S}} u_{\mathcal{S}} + u_{\mathcal{S}} + \partial_{\boldsymbol{n}} u_B = f_{\mathcal{S}}, \quad \text{on } \mathcal{S}, \tag{3}$$

for some constants $\alpha, \beta > 0$. The subscripts B and $\mathcal{S}$ respectively indicate the bulk domain and the boundary used for the coupled equations. The functions in (1)–(3) are $u_B : \Omega \to \mathbb{R}$ and $u_{\mathcal{S}} : \mathcal{S} \to \mathbb{R}$. The source terms f_B and $f_{\mathcal{S}}$ are given in Ω, and $g_{\mathcal{S}}$ is on $\mathcal{S}$. Generally, $g_{\mathcal{S}} = 0$ is set as in [1,2,7].

In (1), ∇ and Δ denote the standard gradient and the Laplace operator in $\mathbb{R}^d$ respectively. Let $\boldsymbol{n}$ be the unit outward normal vector on $\mathcal{S}$, and the normal derivative in (2) is $\partial_{\boldsymbol{n}} := \boldsymbol{n} \cdot \nabla$. Based on the identity matrix I_d of size $d \times d$, the surface gradient $\nabla_{\mathcal{S}}$ is defined by $\nabla_{\mathcal{S}} := (I_d - \boldsymbol{n}\boldsymbol{n}^T)\nabla$, and the Laplace-Beltrami operator is $\Delta_{\mathcal{S}} := \nabla_{\mathcal{S}} \cdot \nabla_{\mathcal{S}}$.

3 Discrete settings, kernels and trial spaces

We will introduce discrete settings, kernels and trial spaces defined in Ω and on $\mathcal{S}$ respectively.

3.1 Discrete settings

For some region $\Pi \in \{\Omega, \mathcal{S}\}$ and given any discrete set of points $\Xi \subset \Pi$, let $dist_\Omega := \|\cdot\|_2$ and $dist_{\mathcal{S}}$ be the Euclidean and geodesic measures in Ω and on $\mathcal{S}$ correspondingly. The *fill distance* h_Ξ and the *separation distance* q_Ξ are defined as

$$h_\Xi := \sup_{\zeta \in \Pi} \inf_{\eta \in \Xi} dist_\Pi(\zeta, \eta) \quad \text{and} \quad q_\Xi := \frac{1}{2} \inf_{\eta^i \neq \eta^j \in \Xi} dist_\Pi(\eta^i, \eta^j). \tag{4}$$

The *mesh ratio* of the set Ξ is defined as $\rho_\Xi := h_\Xi / q_\Xi$.

3.2 Kernels

In this work, we require two kinds of kernels: bulk (or global) kernels $\Phi_{\mu_B} : \mathbb{R}^d \times \mathbb{R}^d \to \mathbb{R}$ of smoothness order μ_B used in bulks, and surface (or restricted) kernels $\Psi_{\mu_{\mathcal{S}}} : \mathcal{S} \times \mathcal{S} \to \mathbb{R}$ of order $\mu_{\mathcal{S}}$ on surfaces $\mathcal{S}$.

The bulk kernel Φ_{μ_B} needs to be symmetric positive definite and its Fourier transform $\hat{\Phi}_{\mu_B}$ satisfies the following decay condition:

$$\hat{\Phi}_{\mu_B}(\boldsymbol{\omega}) \sim (1 + \|\boldsymbol{\omega}\|_2^2)^{-\mu_B}, \tag{5}$$

for all $\boldsymbol{\omega} \in \mathbb{R}^d$. In this case, Φ_{μ_B} can reproduce the standard Hilbert space $\mathcal{H}^{\mu_B}(\Omega)$ provided that Ω is smooth enough if $\mu_B > d/2$. Two examples are the

standard Whittle-Matérn-Sobolev kernels [14] and the Wendland compactly supported kernels [21].

We can suppose that the surface kernels $\Psi_{\mu_\mathcal{S}}$, by restricting Φ_{μ_B} satisfying (5) on $\mathcal{S}$, take the form of

$$\Psi_{\mu_\mathcal{S}}(\cdot\,,\,\cdot) := \Phi_{\mu_B}(\cdot\,,\,\cdot)_{|\mathcal{S}\times\mathcal{S}}, \tag{6}$$

which reproduces $\mathcal{H}^{\mu_\mathcal{S}}(\mathcal{S})$ with $\mu_B = \mu_\mathcal{S} + codim(\mathcal{S})/2 > d/2$, see [4, Assumption 4] and [8,16].

3.3 Bulk and surface trial spaces

To derive some collocation methods for (1)–(3), we respectively distribute scattered points, namely *trial centers* and *collocation points*, both in the domain and on the boundary. With subscripts Ω and $\mathcal{S}$ indicating regions, we employ two sets of centers: $Z_\Omega \subset \Omega$ and $Z_\mathcal{S} \subset \mathcal{S}$, and another three sets of collocations: $X_\Omega \subset \Omega$ and $Y_\mathcal{S} \subset \mathcal{S}$ for the boundary condition (2), and $X_\mathcal{S}$ for the surface equation (3). The points in sets X and Y are used to provide collocation conditions in the numerical least-squares solutions in (17). The centers in set Z are for defining some RBF finite-dimensional spaces, in which we seek for solutions in (9) and (10). Together, we yield resultant matrices of size $(n_X + n_Y) \times n_Z$.

We usually set $Z_\mathcal{S} = Y_\mathcal{S}$. Besides, we also need some assumptions for all these point sets as below.

Assumption 2 *For any region $\Pi \in \{\Omega, \mathcal{S}\}$, let $X = \{\boldsymbol{x}^1, \ldots, \boldsymbol{x}^{n_X}\} \subset \Pi$ and $Y = \{\boldsymbol{y}^1, \ldots, \boldsymbol{y}^{n_Y}\} \subset \mathcal{S}$ be two sets of collocation points, and $Z = \{\boldsymbol{z}^1, \ldots, \boldsymbol{z}^{n_Z}\} \subset \Pi$ be the set of trial centers, respectively. We assume all of them are quasi-uniform, that is, they satisfy*

$$q_\Xi \le h_\Xi \le \rho_\Xi q_\Xi, \quad \Xi \in \{X, Y, Z\} \tag{7}$$

for some constants $\rho_\Xi \ge 1$, and

$$h_Z \le \gamma_{\Xi'} h_{\Xi'}, \quad \Xi' \in \{X, Y\} \subset \Pi, \tag{8}$$

with $Z \subset \Omega$ for some $\gamma_{\Xi'} > 1$ so that Z is denser than Ξ'.

The original Kansa method only requires one set of centers, i.e., $\gamma_{\Xi'} = 1$. In this work, we focus on oversampling conditions, i.e., $\gamma_{\Xi'} > 1$, that yield overdetermined resultant matrices. The quasi-uniform property is needed for all scattered points both in our theoretical analysis and in numerical simulations.

Based on trial centers in Z_Ω or $Z_\mathcal{S}$ and smooth kernels Φ_{μ_B} or $\Psi_{\mu_\mathcal{S}}$ defined in Section 3.2 for bulk domains and surfaces, we can give the following trial spaces correspondingly for interpolation theories to apply.

Firstly, if we solely solve the second-order elliptic problem (1)–(2) in the bulk domain, we can seek numerical approximations from the *bulk trial space* of

translation-invariant kernels Φ_{μ_B} centered at some set of trial centers $Z_\Omega \subset \Omega$ given by

$$\mathcal{U}_{Z_\Omega,\Omega,\Phi_{\mu_B}} := \operatorname{span}\{\Phi_{\mu_B}\left(\cdot - \boldsymbol{z}^j\right) \mid \boldsymbol{z}^j \in Z_\Omega\}. \tag{9}$$

Secondly, when just looking for a numerical solution to the surface PDE (3), we will analyze it in the *surface trial space*

$$\mathcal{U}_{Z_\mathcal{S},\mathcal{S},\Psi_{\mu_\mathcal{S}}} := \operatorname{span}\{\Psi_{\mu_\mathcal{S}}\left(\cdot - \boldsymbol{z}^j\right) \mid \boldsymbol{z}^j \in Z_\mathcal{S}\}. \tag{10}$$

for $Z_\mathcal{S} \subset \mathcal{S}$ by using surface-restricted kernels $\Psi_{\mu_\mathcal{S}}$ in (6).

4 Convergence result for bulk PDEs with Robin boundary conditions

In this section, we will consider

$$\begin{aligned} \mathcal{L}u_B &= f_B, \quad \text{in } \Omega, \\ \mathcal{B}u_B &= g_\mathcal{S}, \quad \text{on } \mathcal{S}, \end{aligned} \tag{11}$$

where $\mathcal{L}$ is a general second-order strongly elliptic operator in Ω, and $\mathcal{B}$ is a Robin boundary operator. The subscript of u_B indicates that the function corresponds to the bulk PDE (11), and subscript B in f_B or $\mathcal{S}$ in $g_\mathcal{S}$ infers the correspondence to the bulk or the surface in the PDE.

Assumption 3 *Assume that $\mathcal{L}$ in* (11) *is second-order strongly elliptic with coefficients in $\mathcal{W}_\infty^{\mu_B-2}(\Omega)$, and coefficients of the Robin boundary operator $\mathcal{B}$ belongs to $\mathcal{W}_\infty^{\mu_B-1}(\mathcal{S})$ on $\mathcal{S}$ of class $\mathcal{C}^{\mu_B}$. Also, we assume that functions f_B and $g_\mathcal{S}$ are smooth enough to admit a classical solution $u_B^* \in \mathcal{H}^{\mu_B}(\Omega)$ to* (11) *for some $\mu_B \geq 2$.*

Since these two operators are bounded, see Assumption 3, we have

$$\|\mathcal{L}u_B\|_{\mathcal{H}^{\nu-2}(\Omega)} \leq C_{\Omega,\mathcal{L}}\|u_B\|_{\mathcal{H}^\nu(\Omega)}, \tag{12}$$

and

$$\|\mathcal{B}u_B\|_{\mathcal{H}^{\nu-3/2}(\mathcal{S})} \leq C_{\mathcal{S},\mathcal{B}}\|u_B\|_{\mathcal{H}^{\nu-1/2}(\mathcal{S})}, \tag{13}$$

for all $u_B \in \mathcal{H}^\nu$ with an integer $\nu \geq 2$ by [10]. For all $u_B \in \mathcal{H}^{\mu_B}(\Omega)$, the following Robin-type boundary regularity estimate holds [20]:

$$\|u_B\|_{\mathcal{H}^\nu(\Omega)} \leq C_{\Omega,\mathcal{L},\nu}(\|\mathcal{L}u_B\|_{\mathcal{H}^{\nu-2}(\Omega)} + \|\mathcal{B}u_B\|_{\mathcal{H}^{\nu-3/2}(\mathcal{S})}), \quad 2 \leq \nu \leq \mu_B, \tag{14}$$

for some constant $C_{\Omega,\mathcal{L},\nu}$ depending only on Ω, $\mathcal{L}$ and ν.

The analysis of error estimates for the Robin-type problem (11) is similar to [6] for Dirichlet PDEs. We can propose the following convergence theorem for this weighted least squares (WLS) solution

$$\begin{aligned} U_B &= U_B^{WLS} \\ &:= \underset{u_B \in \mathcal{U}_{Z_\Omega,\Omega,\Phi_{\mu_B}}}{\arg\inf} \left(\|\mathcal{L}(u_B - u_B^*)\|_{\ell_2(X_\Omega)}^2 + W_\theta\|\mathcal{B}(u_B - u_B^*)\|_{\ell_2(Y_\mathcal{S})}^2\right)^{1/2} \end{aligned} \tag{15}$$

in the bulk trial space $\mathcal{U}_{Z_\Omega,\Omega,\Phi_{\mu_B}}$ in (9), related to a weighting W_θ defined as

$$W_\theta = (h_{Y_\mathcal{S}}/h_{X_\Omega})^{\theta(d/2-\nu+2)} h_{Y_\mathcal{S}}^{-\theta},$$

for $h_{X_\Omega} \le h_{Y_\mathcal{S}} < 1$ and any $0 \le \theta \le 2$.

Theorem 1 *(WLS estimate). Let $\mu_B - d/2 - 1 \ge \nu \ge \max\{2, \lceil d+1 \rceil/2\}$ and $u_B^* \in \mathcal{H}^{\mu_B}(\Omega)$ denote the classical solution to the bulk PDE* (11)*. We assume that all Assumptions 1–3 hold and a kernel Φ_{μ_B} satisfies* (5)*. The discrete sets X_Ω, $Y_\mathcal{S}$ and Z_Ω also yield the condition* (16) *and $h_{X_\Omega} \le h_{Y_\mathcal{S}} < 1$. Then the error estimate of the WLS solution $U_B \in \mathcal{U}_{Z_\Omega,\Omega,\Phi_{\mu_B}}$*

$$\|U_B - u_B^*\|_{\mathcal{H}^\nu(\Omega)} \le C_{\Omega,\mathcal{S},\mathcal{L},\mathcal{B},\Phi_{\mu_B},\nu,\rho_{X_\Omega},\rho_{Y_\mathcal{S}},\gamma_{X_\Omega},\gamma_{Y_\mathcal{S}}} (h_{Z_\Omega}^{\theta/2-1}+1) h_{Z_\Omega}^{\mu_B-\nu} \|u_B^*\|_{\mathcal{H}^{\mu_B}(\Omega)},$$

holds for $0 \le \theta \le 2$, and a positive constant C depending on $\Omega, \mathcal{S}, \mathcal{L}, \mathcal{B}, \Phi_{\mu_B}, \nu$, $\rho_{X_\Omega}, \rho_{Y_\mathcal{S}}, \gamma_{X_\Omega}$ and $\gamma_{Y_\mathcal{S}}$, provided that the sets of trial centers $Z_\Omega \subset \Omega$ and collocation points $X_\Omega \subset \Omega$ and $Y_\mathcal{S} \subset \mathcal{S}$ satisfy the oversampling condition

$$C_{\Omega,\mathcal{S},\mathcal{L},\mathcal{B},\Phi_{\mu_B},\nu} (h_{X_\Omega}^{\mu_B-\nu} + h_{Y_\mathcal{S}}^{\mu_B-\nu}) q_{Z_\Omega}^{-\mu_B+\nu} < \frac{1}{2}, \tag{16}$$

to ensure stability for some constant $C_{\Omega,\mathcal{S},\mathcal{L},\mathcal{B},\Phi_{\mu_B},\nu} > 0$ independent of X_Ω.

Proof. Based on the regularity inequality in (14) for Robin boundary conditions, we can follow the same proof of the convergence theorem for the least-squares solutions to Dirichlet problems in [6]. □

We remark that, in theory, both $h_{X_\Omega} \sim h_{Z_\Omega}/4$ and $h_{Y_\mathcal{S}} \sim h_{Z_\Omega}/4$ are required for (16) to hold for the problem in (11). To identify the practical requirement, we will verify this oversampling condition both in Ω and on $\mathcal{S}$ in Example 6.1.1.

5 Meshless collocation methods for coupled bulk-surface PDEs

We will solve the coupled problem in (1)–(3) for the solutions $(u_B, u_\mathcal{S})$ by a domain-type meshless collocation method in [6] and an intrinsic surface-type approach in [4]. Our method is based on the coupled trial space $\mathcal{U}_{Z_\Omega,\Omega,\Phi_{\mu_B}} \times \mathcal{U}_{Z_\mathcal{S},\mathcal{S},\Psi_{\mu_\mathcal{S}}}$ in (9) and (10). For simplicity, we will use the simplest version of the WLS estimate in Theorem 1 without weightings. We will identify our least-squares solutions $(U_B, U_\mathcal{S})$, defined by

$$\underset{\substack{u_B \in \mathcal{U}_{Z_\Omega,\Omega,\Phi_{\mu_B}} \\ u_\mathcal{S} \in \mathcal{U}_{Z_\mathcal{S},\mathcal{S},\Psi_{\mu_\mathcal{S}}}}}{\arg\inf} \Big(\|\mathcal{L}u_B - f_B\|_{\ell_2(X_\Omega)}^2 + \|\mathcal{B}u_B - \beta u_\mathcal{S} - g_\mathcal{S}\|_{\ell_2(Y_\mathcal{S})}^2 \tag{17}$$

$$+ \|\mathcal{L}_\mathcal{S} u_\mathcal{S} + \partial_{\boldsymbol{n}} u_B - f_\mathcal{S}\|_{\ell_2(X_\mathcal{S})}^2 \Big),$$

where $\mathcal{L} := -\Delta + I_d$ and $\mathcal{B} := \alpha + \partial_{\boldsymbol{n}}$, and the strongly second-order elliptic operator $\mathcal{L}_\mathcal{S} := -\Delta_\mathcal{S} + I_d$ is imposed on the boundary, as well as $Z_\Omega \subset \Omega$, $X_\Omega \subset \Omega$, and $\{Z_\mathcal{S}, Y_\mathcal{S}, X_\mathcal{S}\} \subset \mathcal{S}$.

5.1 Implementation

Before introducing how to implement our meshless collocation methods for the coupled bulk-surface PDEs (1)–(3), we will give a general linear expansion of trial functions either in the domain or on the surface by

$$I_Z u = \sum_{i=1}^{n_Z} \lambda_i \Theta\left(\cdot, \boldsymbol{z}^i\right), \quad \boldsymbol{z}^i \in Z, \tag{18}$$

where $Z = Z_\Omega \subset \Omega$, $\lambda = \lambda_B$ and $\Theta = \Phi_{\mu_B}$ for $u = u_B$ in the bulk, and $Z = Z_\mathcal{S} \subset \mathcal{S}$, $\lambda = \lambda_\mathcal{S}$ and $\Theta = \Psi_{\mu_\mathcal{S}}$ for $u = u_\mathcal{S}$ on the boundary. For numerical stability, $n_X > n_Z$ is required for Ω and $\mathcal{S}$ and we give an example in Figure 1. Note that all surface points are quasi-uniform expect those in the unit ball that indeed uniform.

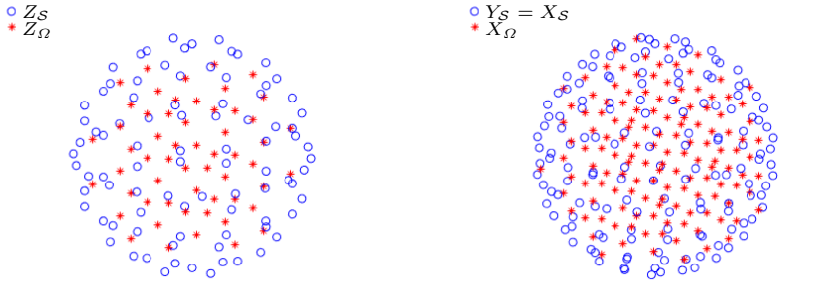

(a) Trial centers
$n_{Z_\mathcal{S}} = 88$, $n_{Z_\Omega} = 56$

(b) Collocation points
$n_{X_\mathcal{S}} = n_{Y_\mathcal{S}} = 150$, $n_{X_\Omega} = 136$

Fig. 1 The quasi-uniform distribution of trial centers and collocations in the unit ball and on its boundary.

In matrix form, based on the expressions $I_{Z_\Omega} u_B$ and $I_{Z_\mathcal{S}} u_\mathcal{S}$ in (18), we respectively impose collocation conditions in the bulk and on the surface elliptic operators: $\mathcal{L}$ in (1) and $\mathcal{L}_\mathcal{S}$ in (3), as well as the Robin boundary operator $\mathcal{B}$ in (2). Thus, we have

$$\begin{cases} [L]_{ij} &= \mathcal{L}\Phi_{\mu_B}(\boldsymbol{x}^i, \boldsymbol{z}^j) & \boldsymbol{x}^i \in X_\Omega, \boldsymbol{z}^j \in Z_\Omega, \\ [L_\mathcal{S}]_{ij} &= \mathcal{L}_\mathcal{S}\Psi_{\mu_\mathcal{S}}(\boldsymbol{x}^i, \boldsymbol{z}^j) & \boldsymbol{x}^i \in X_\mathcal{S}, \boldsymbol{z}^j \in Z_\mathcal{S}, \\ [B_n]_{ij} &= \sum_{k=1}^{d} n_k(\boldsymbol{x}^i)\Big(\partial_{x_k}\Phi_{\mu_B}(\boldsymbol{x}^i, \boldsymbol{z}^j)\Big) & \boldsymbol{x}^i \in \{Y_\mathcal{S}, X_\mathcal{S}\}, \boldsymbol{z}^j \in Z_\Omega \\ [K_B]_{ij} &= \Phi_{\mu_B}(\boldsymbol{x}^i, \boldsymbol{z}^j) & \boldsymbol{x}^i \in \{X_\Omega, Y_\mathcal{S}\}, \boldsymbol{z}^j \in Z_\Omega, \\ [K_\mathcal{S}]_{ij} &= \Psi_{\mu_\mathcal{S}}(\boldsymbol{x}^i, \boldsymbol{z}^j) & \boldsymbol{x}^i \in \{Y_\mathcal{S}, X_\mathcal{S}\}, \boldsymbol{z}^j \in Z_\mathcal{S}. \end{cases} \tag{19}$$

As a result, we can assemble all matrices in (19) into the following system of equations for the PDEs (1)–(3):

$$\begin{array}{c} \\ X_\Omega \\ Y_\mathcal{S} \\ X_\mathcal{S} \end{array} \begin{array}{c} \begin{array}{ccc} Z_\Omega & & Z_\mathcal{S} = Y_\mathcal{S} \end{array} \\ \begin{bmatrix} L & & \mathbf{0} \\ \alpha K_B + B_n & & -\beta K_\mathcal{S} \\ B_n & & L_\mathcal{S} \end{bmatrix} \end{array} \begin{bmatrix} \lambda_B \\ \lambda_\mathcal{S} \end{bmatrix} = \begin{bmatrix} f_{B|X_\Omega} \\ g_{\mathcal{S}|Y_\mathcal{S}} \\ f_{\mathcal{S}|X_\mathcal{S}} \end{bmatrix}, \tag{20}$$

and then solve it for the unknown coefficients λ_B and $\lambda_\mathcal{S}$ to interpolate the corresponding least-squares approximations U_B and $U_\mathcal{S}$ to (17).

5.2 Some discussions on convergence

Based on the theoretical analyses of the bulk and the surface-type collocation methods respectively, we can split the system (1)–(3) into a bulk PDE with a Robin boundary condition by replacing $g_\mathcal{S}$ in (11) with $(g_\mathcal{S} + \beta u^*_\mathcal{S})$:

$$\begin{array}{ll} \mathcal{L}u_B = f_B, & \text{in } \Omega, \\ \mathcal{B}u_B = g_\mathcal{S} + \beta u^*_\mathcal{S}, & \text{on } \mathcal{S}, \end{array} \tag{21}$$

and an elliptic PDE on the surface:

$$\mathcal{L}_\mathcal{S} u_\mathcal{S} = f_\mathcal{S} - \partial_{\boldsymbol{n}} u^*_B, \quad \text{on } \mathcal{S}, \tag{22}$$

where $\mathcal{L}_\mathcal{S}$ satisfies the boundedness as follows.

Assumption 4 *Assume that $\mathcal{L}_\mathcal{S}$ is second-order strongly elliptic on $\mathcal{S}$ whose coefficients are in $\mathcal{W}^{\mu_\mathcal{S}-2}_\infty(\mathcal{S})$, and $f_\mathcal{S}$ is smooth enough to admit a classical solution $u^*_\mathcal{S} \in \mathcal{H}^{\mu_\mathcal{S}}(\mathcal{S})$ to (22) for some $\mu_\mathcal{S} \geq 2$.*

Since we now have two PDEs in the domain and on the boundary respectively, we consider them together from two aspects. On the one hand, we can mainly research on the bulk estimate for (21), and take the surface error as a perturbation of $u^*_\mathcal{S}$ on the boundary. On the other hand, the surface solution to (22) reversely is regarded as our primary consideration with a right hand side perturbation from u^*_B.

5.2.1 Theoretical requirements for smoothness of kernels

For approximations in the bulk and on the surface, there are different theoretical conditions of smoothness orders μ_B for the global kernel Φ_{μ_B} and $\mu_\mathcal{S}$ for the restricted one $\Psi_{\mu_\mathcal{S}}$.

We firstly focus on the bulk-domain problem (21), provided that a known least-square numerical approximation $u^*_\mathcal{S} \approx U_\mathcal{S}$ obtained by (22) with the exact right hand side. The bulk estimate of an error $(U_B - u^*_B)$ is in the Sobolev norm up to the order $\nu \leq \mu_B$, as well as an extra perturbation $\epsilon_\mathcal{S} = U_\mathcal{S} - u^*_\mathcal{S}$ in the $\mathcal{H}^{\nu-3/2}(\mathcal{S})$ norm from the boundary regularity term in (14). By using

Theorem 1 solely for the bulk PDE (21), we require $\mu_B - d/2 - 1 \geq \nu \geq \max\{2, \lceil d+1 \rceil/2\}$. Further, $\mu_{\mathcal{S}} \geq \lceil \nu + d_{\mathcal{S}}/2 - 1/2 \rceil$ and $\nu \geq 3.5$ are essential in terms of the $\mathcal{H}^{\nu-3/2}(\mathcal{S})$ error only for the surface PDE (22), see [4]. Therefore, in this case, we need

$$\begin{cases} \mu_B \geq \nu + d/2 + 1, \\ \mu_{\mathcal{S}} \geq \lceil \nu + d_{\mathcal{S}}/2 - 1/2 \rceil, \end{cases} \quad \text{for } \nu \geq 3.5. \tag{23}$$

Reversely, the error $(U_{\mathcal{S}} - u_{\mathcal{S}}^*)$ in the $\mathcal{H}^k(\mathcal{S})$ norm is primarily considered, then $\mu_{\mathcal{S}} \geq \lceil k + d_{\mathcal{S}}/2 + 1 \rceil$ is needed for all $k \geq 2$. Besides, we assume that the right hand side in (22) is obtained by $u_B^* \approx U_B$, so that the error $\epsilon_B = \partial_{\boldsymbol{n}}(U_B - u_B^*)$ is approximately in $\mathcal{H}^{k-2}(\mathcal{S})$ according to the regularity in [4, Lemma 3.1]. Because of the bounded $\partial_{\boldsymbol{n}}$ and the trace theorem [22], we have

$$\|\epsilon_B\|_{\mathcal{H}^{k-2}(\mathcal{S})} \leq C_{\boldsymbol{n}} \|(U_B - u_B^*)_{|\mathcal{S}}\|_{\mathcal{H}^{k-1}(\mathcal{S})} \leq C_{\boldsymbol{n}} \|U_B - u_B^*\|_{\mathcal{H}^{k-1/2}(\Omega)}, \tag{24}$$

for $\mu_B \geq k + d/2 + 1/2$ and $k \geq 2.5$ theoretically. As a result,

$$\begin{cases} \mu_B \geq k + d/2 + 1/2, \\ \mu_{\mathcal{S}} \geq \lceil k + d_{\mathcal{S}}/2 + 1 \rceil, \end{cases} \quad \text{for } k \geq 2.5. \tag{25}$$

By a comparison between (23) and (25), the latter one has lower requirements for the orders of both kernels in theory.

5.2.2 Selections of bulk and surface orders of smoothness

In the coming part, we will discuss convergence also from two aspects under the basic smoothness conditions (23) and (25) based on existing theoretical error outcomes respectively.

For the bulk PDE (21) with a perturbation of $u_{\mathcal{S}}^*$, we can consider two parts. The first part $\|U_B - u_B^*\|_{\mathcal{H}^\nu(\Omega)}$ converges to

$$h_{Z_\Omega}^{\mu_B - \nu} \|u_B^*\|_{\mathcal{H}^{\mu_B}(\Omega)},$$

by using Theorem 1 for $\theta = 2$, if using $u_{\mathcal{S}}^*$ for (21). In terms of the second perturbation part $\|\epsilon_{\mathcal{S}}\|_{\mathcal{H}^{\nu-3/2}(\mathcal{S})}$, we can ignore the error from U_B in (22) to approximately obtain by [4, Theorem 1.1]:

$$\|\epsilon_{\mathcal{S}}\|_{\mathcal{H}^{\nu-3/2}(\mathcal{S})} \lesssim C_{\mathcal{S},\mathcal{L}_{\mathcal{S}},\Psi_{\mu_{\mathcal{S}}},\nu,\rho_{Y_{\mathcal{S}}},\gamma_{Y_{\mathcal{S}}}} h_{Z_{\mathcal{S}}}^{\mu_{\mathcal{S}} - \nu - d_{\mathcal{S}}/2 + 3/2} \|u_{\mathcal{S}}^*\|_{\mathcal{H}^{\mu_{\mathcal{S}}}(\mathcal{S})}. \tag{26}$$

To avoid being affected by $\epsilon_{\mathcal{S}}$ for the bulk convergence estimate, we require that the rate of in (26) is not less than $(\mu_B - \nu)$:

$$\mu_{\mathcal{S}} \geq \mu_B + d_{\mathcal{S}}/2 - 3/2, \tag{27}$$

for $\mu_B \geq \nu + d/2 + 1$ with $\nu \geq 3.5$, see (23).

For the surface PDE (22) with a perturbation of u_B^*, the upper bound of $\|U_{\mathcal{S}} - u_{\mathcal{S}}^*\|_{\mathcal{H}^k(\mathcal{S})}$ is obtained by (26):

$$h_{Z_{\mathcal{S}}}^{\mu_{\mathcal{S}} - k - d_{\mathcal{S}}/2} \|u_{\mathcal{S}}^*\|_{\mathcal{H}^{\mu_{\mathcal{S}}}(\mathcal{S})}. \tag{28}$$

In addition, the convergence rate for the bulk perturbation $\|\epsilon_B\|_{\mathcal{H}^{k-2}(\mathcal{S})}$ (or $\|U_B - u_B^*\|_{\mathcal{H}^{k-1/2}(\Omega)}$ from (24)) is $(\mu_B - k + 1/2)$ via Theorem 1 with $\theta = 2$. In order to reach the convergence rate in (28), it is essential to set

$$\mu_B \geq \mu_{\mathcal{S}} - d_{\mathcal{S}}/2 - 1/2. \tag{29}$$

Since $\mu_B \geq k + d/2 + 1/2$ by (25), $\mu_{\mathcal{S}} - d_{\mathcal{S}}/2 - 1/2 \geq k + d/2 + 1/2$, that is, $\mu_{\mathcal{S}} \geq k + (d + d_{\mathcal{S}})/2 + 1$ with $k \geq 2.5$.

Note that requirements for smoothness orders μ_B and $\mu_{\mathcal{S}}$, under (27) and (29), are stronger than those in (23) and (25) respectively. But (29) is better, due to the high-order convergence performance of the intrinsic surface approach in [4]. Later, we will confirm this numerically in Section 6.1.

6 Numerical experiments

We implement the proposed meshless collocation method in Section 5.1 with the Whittle-Matérn-Sobolev kernels of various smoothness orders μ_B for bulk approximation and the restricted ones of order $\mu_{\mathcal{S}}$ on surfaces. For discretization, trial centers and collocation points are usually different but are uniformly scattered in domains and on surfaces. Here, we use the same sets of points for collocations $Y_{\mathcal{S}}$ and $X_{\mathcal{S}}$ on boundaries. For brevity, we give some simplified notations with subscripts for fill distances h of these points in the following cases:

$$\begin{cases} h_{\Pi} = h_{X_{\Pi}} = h_{Z_{\Pi}} & \text{for } X_{\Pi} = X_{\Pi}, \text{ and } \Pi \in \{\Omega, \mathcal{S}\}, \\ h_{\Xi} = h_{\Xi_{\Omega}} = h_{\Xi_{\mathcal{S}}} & \text{for } \Xi_{\Omega} = \Xi_{\mathcal{S}}, \text{ and } \Xi \in \{X, Z\}. \end{cases}$$

The number n of points in any set is subscripted in the same way.

Section 6.1 presents two studies of effects of smoothness orders of kernels on the accuracy and convergence. In the first example, we set different fill distances for two classes of points in X and Z. The second test also compares our proposed method with two FEMs. The cut FEM approximated both the embedded domain and numerical solutions to the coupled bulk-surface problems [2]. Another FEM used piece-wise polynomial finite element functions on a polyhedral approximation of the domain [7]. In Section 6.2, we show the resulting estimates via discretizing the domain and its boundary under different denseness of point sets. Lastly in Section 6.3, we impose three distinct types of source terms to (1)–(3) in two domains.

6.1 Smoothness orders of kernels for accuracy and convergence

As discussed in Section 5.2, from the aspects for the bulk and the surface convergence, the theoretical requirements and the relationships between smoothness orders μ_B and $\mu_{\mathcal{S}}$ of kernels are different. Here, we seek how to balance these two orders numerically in the following experiments.

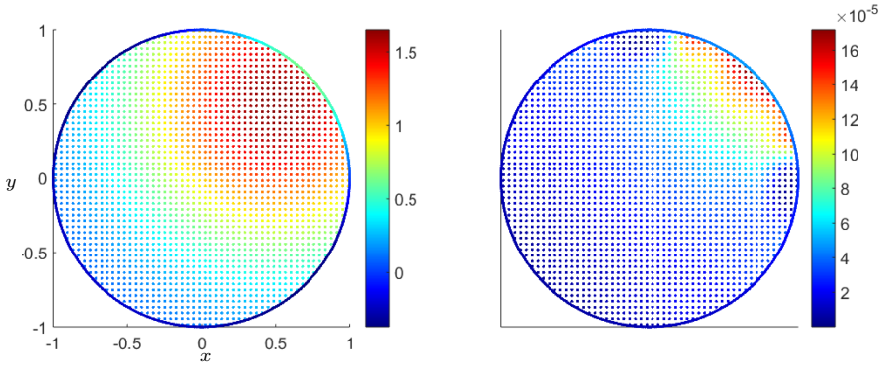

(a) Numerical solutions (b) Error functions

Fig. 2 Example 6.1.1: The numerical solutions and error functions (color) in the unit disk and on its boundary, obtained by the surface kernel of order $\mu_{\mathcal{S}} = 4.5$ and the bulk kernel of $\mu_B = 5$, using the same $X = Z$ for bulk and boundary respectively, and $n_\Omega = 104$ points inside and $n_{\mathcal{S}} = 36$ on the boundary with $h_\Omega = h_{\mathcal{S}} = 0.0304$.

We let the classical solutions to (1)–(3) with $\alpha = \beta = 1$ be

$$\begin{aligned} u_B^* &= e^{-x(x-1)-y(y-1)}, \\ u_{\mathcal{S}}^* &= (1 + x(1-2x) + y(1-2y))e^{-x(x-1)-y(y-1)}. \end{aligned} \tag{30}$$

All source terms of the right hand sides in (1)–(3) can be analytically derived. Particularly, we have $g_{\mathcal{S}} = 0$ in the unit disk and the unit ball for (30).

Example 6.1.1 ***In the unit disk in*** $\mathbb{R}^2$**.** We firstly apply our coupled method to solve the problem (1)–(3) in the unit disk with $\mu_B = 5$ and $\mu_{\mathcal{S}} = 4.5$. The trial centers and collocations are identically distributed in Ω and on $\mathcal{S}$ with the same fill distance $h = 0.0304$. In Figure 2, the corresponding numerical solutions and their error functions are plotted.

Table 1(a)–(b) lists the L^2 errors of the bulk and surface solutions with varieties of smoothness orders μ_B and $\mu_{\mathcal{S}}$. In the part (a) of Table 1, with increasing $\mu_{\mathcal{S}}$ associated with a minimum $\mu_B = 5.5$ required by (27) in theory, the bulk solutions are almost as accurate as those on the surface. Reversely, under a lowest condition $\mu_{\mathcal{S}} = 5$ by (29), Table 1(b) shows that raising μ_B can obviously decrease both $L^2(\Omega)$ and $L^2(\mathcal{S})$ errors. We use $\mu_{\mathcal{S}} = 3.5$ in (a) and $\mu_B = 3.5$ in (b) that are even smaller than basically theoretical requirements in (23) and (25) respectively. The corresponding L^2 accuracies are still high in comparison with others using higher-order kernels. The results here suggest that kernels with lower than theoretical required smoothness can still be practical despite the lack of error bounds. We also find that errors on the circle are smaller than those inside under the same point densities for all set points.

(Oversampling settings) Next, we test how much denser collocation points in X have to be with respect to the centers in Z, respectively in the bulk and on the circle. We fix kernels of orders $\mu_B = \mu_{\mathcal{S}} = 5$, and $h_Z = h_{Z_\Omega} = h_{Z_{\mathcal{S}}}$

Table 1 Example 6.1.1: The L^2 errors in a unit disk and on its boundary, obtained by (a) a fixed μ_B with various $\mu_{\mathcal{S}}$ and (b) a fixed $\mu_{\mathcal{S}}$ with various μ_B, using the same setting: $X = Z$ for the bulk and the boundary and $n_\Omega = 104$ in Ω and $n_{\mathcal{S}} = 36$ on $\mathcal{S}$ ($h_\Omega = h_{\mathcal{S}} = 0.0304$).

(a) Bulk $\mu_B = 5.5$	$\mu_{\mathcal{S}}$				
	3.5	4.5	5	5.5	6
$L^2(\Omega)$	4.28344E-05	4.29578E-05	4.29582E-05	4.29583E-05	4.29583E-05
$L^2(\mathcal{S})$	1.52230E-05	1.57156E-05	1.57175E-05	1.57176E-05	1.57176E-05
(b) Surface $\mu_{\mathcal{S}} = 5$	μ_B				
	3.5	4	4.5	5	6
$L^2(\Omega)$	1.46683E-03	2.97756E-04	1.92086E-04	8.18739E-05	2.38069E-05
$L^2(\mathcal{S})$	7.40532E-04	1.26852E-04	1.01760E-04	4.11273E-05	7.43383E-06

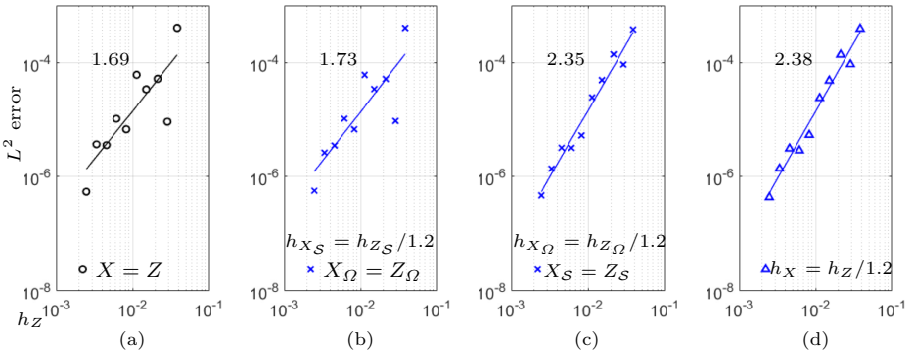

Fig. 3 Example 6.1.1: The convergence profiles of L^2 errors both in the unit disk and on the boundary, obtained by fixing $\mu_B = \mu_{\mathcal{S}} = 5$ for two kernels, using different oversampling settings: (a) $X = Z$; (b) only denser $X_{\mathcal{S}}$ with $h_{X_{\mathcal{S}}} = h_{Z_{\mathcal{S}}}/1.2$ on $\mathcal{S}$; (c) only denser X_Ω with $h_{X_\Omega} = h_{Z_\Omega}/1.2$ in Ω; (d) $h_X = h_Z/1.2$ for all points.

for two sets of centers. In Figure 3, by employing $X = Z$ and three oversampling settings, we show the corresponding L^2 convergence profiles. More collocation points with the ratio $h_Z/h_X = 1.2$ in Ω can increase convergence rate from 1.7 to 2.4. When higher oversampling ratio $h_Z/h_X = 1.5$ is applied, see Figure 4(a), we find no clear benefits in terms of both accuracy and convergence rate. By increasing smoothness orders of the kernels to $\mu_B = \mu_{\mathcal{S}} = 6$, Figure 4(b) illustrates better L^2 convergence behavior with the rate 3.1. Using higher $\mu_{\mathcal{S}}$ with μ_B fixed does not yield further improvement and we omit the numerical results.

Then we turn to apply different $\mu_B = 4,\ 6$ and 6.5 for the bulk kernels with a fixed $\mu_{\mathcal{S}} = 5$ and the oversampling condition $h_X = h_Z/1.2$. Their L^2 errors are respectively profiled in Figure 5. The corresponding convergence rates between $L^2(\Omega)$ and $L^2(\mathcal{S})$ are similar for each tested μ_B. Besides, the bulk kernels with higher smoothness orders can improve convergence (rates from 1.3 to 2.4 roughly). But solutions via $\mu_B = 6.5$ become less accurate when using the smallest $h_Z = 0.004$, and even worse than results by $\mu_B = 6$.

Therefore, either from accuracy or from convergence, our method run better on surfaces than in domains. That is to say, via (29), it is more effective to vary bulk kernels with surface ones fixed.

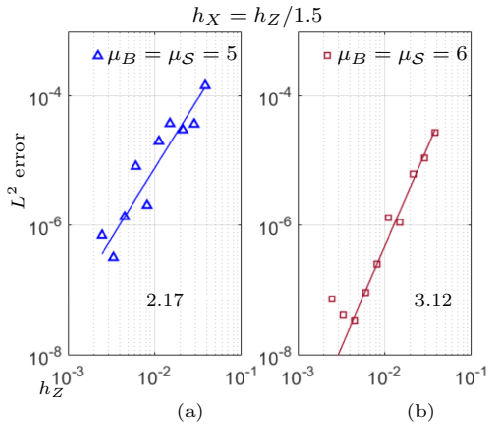

Fig. 4 Example 6.1.1: Under the same oversampling condition $h_X = h_Z/1.5$ for all points, the convergence profiles of L^2 errors both in the unit disk and on the boundary, obtained by respectively fixing (a) $\mu_B = \mu_S = 5$ and (b) $\mu_B = \mu_S = 6$ for two kernels.

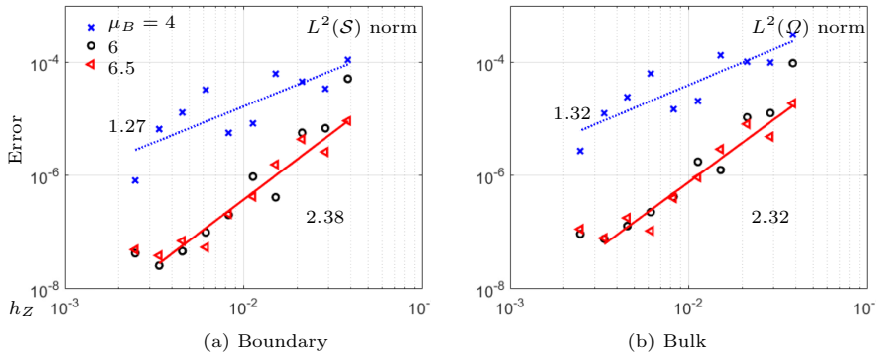

Fig. 5 Example 6.1.1: The convergence profiles of L^2 errors (a) on the boundary and (b) in the unit disk, obtained by fixing boundary kernels of order $\mu_S = 5$ with various μ_B for bulk kernels, using $h_X = h_Z/1.2$ both in the bulk and on the boundary.

Example 6.1.2 ***In the unit ball in*** $\mathbb{R}^3$**.** We consider an example in the unit ball for comparison with the results in [2,7]. Our proposed approach is employed to yield approximated solutions in Figure 6(a) and the error functions in Figure 6(b) with $\mu_S = 6$ and $\mu_B = 6$.

Table 2 shows the L^2 and $\mathcal{H}^1$ errors in the domain and on the boundary when utilizing a minimum requirement $\mu_B = 6$ from (27) with different μ_S respectively. Another test uses a lowest $\mu_S = 6$ via (29) and various μ_B. The results are listed in Table 3. It is observed that increasing the bulk order μ_B in Table 3 is more effective than changing μ_S in Table 2 in terms of accuracy. Although $\mu_S = 3.5$ used in Table 2 is smaller than the essentially theoretical minimum 4, and $\mu_S = 4$ in Table 3 is also less than 5, see (23) and (25). Their outcomes are respectively close to those obtained by higher smoothness

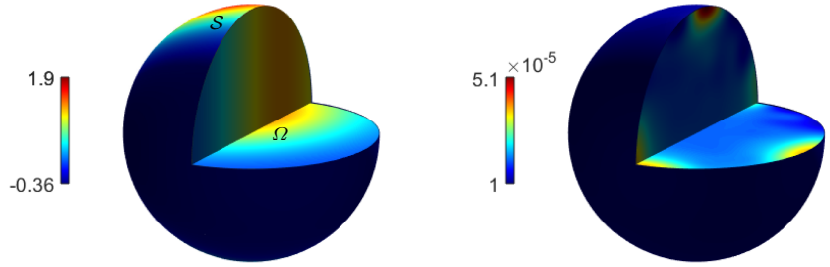

(a) Numerical solutions (b) Error functions

Fig. 6 Example 6.1.2: The numerical solutions and error functions (color) in a ball and on its boundary, obtained by boundary kernels of $\mu_{\mathcal{S}} = 6$ and bulk kernel $\mu_B = 6.5$, using the same $X = Z$ for bulk and boundary respectively, and $n_\Omega = 657$ points inside and $n_{\mathcal{S}} = 409$ on the boundary with $h_\Omega = h_{\mathcal{S}} = 0.0341$.

Table 2 Example 6.1.2: The L^2 and $\mathcal{H}^1$ errors in the unit ball and on the sphere, obtained by fixing orders $\mu_B = 6$ for bulk with various $\mu_{\mathcal{S}}$ for boundary, using the same $X = Z$ for bulk and boundary respectively, and $n_\Omega = 136$ points inside and $n_{\mathcal{S}} = 147$ on the boundary with $h_\Omega = h_{\mathcal{S}} = 0.0988$.

$\mu_B = 6$		$\mu_{\mathcal{S}}$				
		3.5	5.5	6	6.5	7
Ω	L^2	5.8829E-04	6.0051E-04	5.9917E-04	5.9843E-04	5.9800E-04
	$\mathcal{H}^1$	1.9285E-03	2.0039E-03	2.0056E-03	2.0066E-03	2.0071E-03
$\mathcal{S}$	L^2	5.3431E-04	2.2611E-04	2.2282E-04	2.2099E-04	2.1990E-04
	$\mathcal{H}^1$	2.9622E-03	2.7699E-04	2.4271E-04	2.2636E-04	2.1865E-04

Table 3 Example 6.1.2: The L^2 and $\mathcal{H}^1$ errors in the unit ball and on the sphere, obtained by fixing orders $\mu_{\mathcal{S}} = 6$ for boundary with various μ_B for bulk, using the same setting as in Table 2.

$\mu_{\mathcal{S}} = 6$		μ_B				
		4	4.5	5.5	6.5	7.5
Ω	L^2	3.89082E-03	1.98549E-03	1.04391E-03	2.68917E-04	5.96153E-04
	$\mathcal{H}^1$	1.60029E-02	8.09519E-03	3.13674E-03	1.14387E-03	7.03852E-04
$\mathcal{S}$	L^2	1.00351E-03	5.57316E-04	4.21405E-04	7.48756E-05	2.93475E-04
	$\mathcal{H}^1$	1.59783E-03	7.90789E-04	3.26253E-04	1.85107E-04	1.68095E-04

orders. Our method produces the results comparable to those in [2, Figure 4] and [7, Tables 1–2] in terms of L^2 and $\mathcal{H}^1$ errors.

In Figure 7(a)–(d), we give four profiles of $L^2(\mathcal{S})$, $L^2(\Omega)$, $\mathcal{H}^1(\mathcal{S})$ and $\mathcal{H}^1(\Omega)$ errors. They are obtained by employing $\mu_{\mathcal{S}} = 5$ with several $\mu_B = 4,\ 5,\ 7$ and 7.5 under the oversampling setting $n_X > n_Z$. We achieve the higher L^2 and $\mathcal{H}^1$ convergence rates when μ_B goes up. It is enough to use $\mu_B = 7.5$ for $\mu_{\mathcal{S}} = 5$, due to the descend of accuracy with the smallest h_Z in all the sub-figures. Figure 7(c)–(d) show good performance in the $\mathcal{H}^1$ convergence. Consistent with Example 6.1.1 for 2D, the 3D test also verifies that higher μ_B than $\mu_{\mathcal{S}}$ is beneficial to numerical performance. Moreover, our numerical results converge faster with the bulk kernel with the high order $\mu_B = 7.5$ in comparison with those shown in [2] and [7, Tables 3–4].

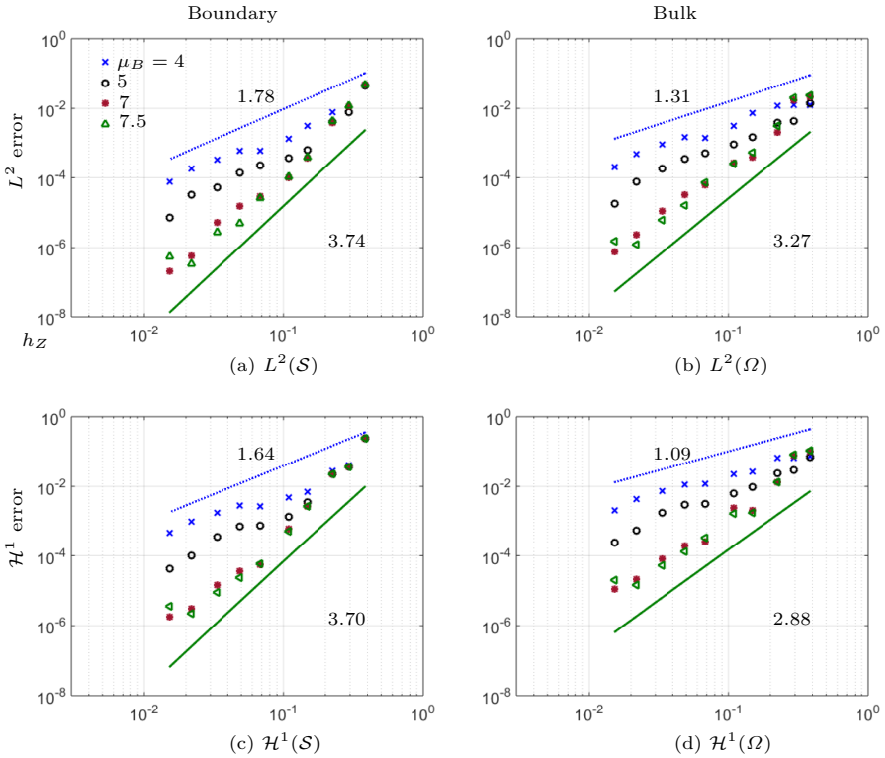

(a) $L^2(\mathcal{S})$ (b) $L^2(\Omega)$ (c) $\mathcal{H}^1(\mathcal{S})$ (d) $\mathcal{H}^1(\Omega)$

Fig. 7 Example 6.1.1: The least-squares convergence profiles of L^2 and $\mathcal{H}^1$ errors on the boundary and in the unit ball (a)–(d), obtained by fixing boundary kernels of order $\mu_{\mathcal{S}} = 5$ with various μ_B for bulk kernels, using $n_{X_{\mathcal{S}}} \approx 200\% n_{Z_{\mathcal{S}}}$ and $n_{X_\Omega} > n_{Z_\Omega}$ with $h_{X_\Omega} = h_{X_{\mathcal{S}}}$ and $h_{Z_\Omega} = h_{Z_{\mathcal{S}}}$.

6.2 Point settings for bulk and surface in a torus

Example 6.2.1 We set the exact solutions as in (30) in a domain surrounded by a torus[1] so that $g_{\mathcal{S}} \neq 0$. Figure 8 shows the numerical solutions and error functions obtained via oversampling $n_X > n_Z$ and kernels with smoothness orders $\mu_B = 5.5$ and $\mu_{\mathcal{S}} = 5$.

For studying how to impose point settings for the bulk and the boundary, we void oversampling collocation points and use $X = Z$ for all discretizations. We respectively use the same fill distance $h_{\mathcal{S}} = 0.1831$ of surface points for four bulk settings $h_\Omega = h_{\mathcal{S}}/\{1, 2, 4, 6\}$, and fix $h_\Omega = 0.0511$ ($n_\Omega = 76$) with various numbers $n_{\mathcal{S}} = \{76, 160, 324, 448\}$ of points on the boundary. The resulting L^2 and $\mathcal{H}^1$ errors are listed in Tables 4 and 5 correspondingly. It can be found that having denser points on the surface instead of bulk points can more effectively improve the L^2 and $\mathcal{H}^1$ accuracy both inside and on the torus. Table 5 shows

[1] $(x^2 + y^2 + z^2 + 1^2 - (1/3)^2)^2 - 4(x^2 + y^2) = 0$.

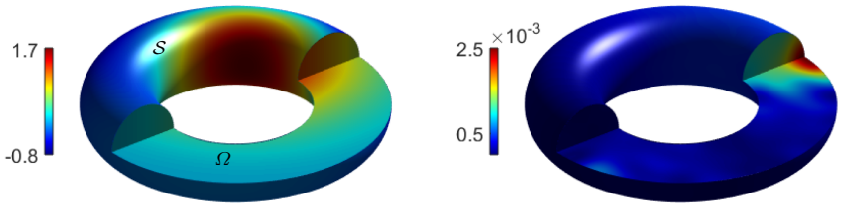

(a) Numerical solutions (b) Error functions

Fig. 8 Example 6.2.1: The numerical solutions and error functions (color) in a Torus and on its boundary, obtained by the boundary kernel with $\mu_{\mathcal{S}} = 5$ and the bulk kernel with $\mu_B = 5.5$, using $(n_{X_\Omega}, n_{Z_\Omega}, n_{X_{\mathcal{S}}}, n_{Z_{\mathcal{S}}}) = (246, 236, 448, 352)$ with $h_X = 0.0444$ and $h_Z = 0.04$.

Table 4 Example 6.2.1: The L^2 and $\mathcal{H}^1$ errors in a torus and on its boundary, obtained by fixing $h_{\mathcal{S}} = 0.1831$ ($n_{\mathcal{S}} = 76$) for surface with various fill distance rates $c = h_{\mathcal{S}}/h_\Omega$ for bulk, using kernels of smoothness orders: $(\mu_B, \mu_{\mathcal{S}}) = (5.5, 5)$ and the same $X = Z$ for bulk and boundary respectively.

c	n_Ω	Bulk		Boundary	
		$L^2(\Omega)$	$\mathcal{H}^1(\Omega)$	$L^2(\mathcal{S})$	$\mathcal{H}^1(\mathcal{S})$
1	24	5.0308E-03	1.5472E-02	7.6386E-03	4.1945E-02
2	77	2.5891E-03	1.0398E-02	7.5352E-03	4.1843E-02
4	235	2.1726E-03	8.2467E-03	7.7691E-03	4.1872E-02
6	434	2.6163E-03	8.9547E-03	7.8436E-03	4.1890E-02

Table 5 Example 6.2.1: The L^2 and $\mathcal{H}^1$ errors in a Torus and on its boundary, obtained by fixing $h_\Omega = 0.0511$ ($n_\Omega = 193$) for bulk with various $h_{\mathcal{S}}$ for surface, using the same settings as in Table 4.

$h_{\mathcal{S}}$	$n_{\mathcal{S}}$	Bulk		Boundary	
		$L^2(\Omega)$	$\mathcal{H}^1(\Omega)$	$L^2(\mathcal{S})$	$\mathcal{H}^1(\mathcal{S})$
0.1831	76	2.2288E-03	1.0056E-02	7.7578E-03	4.1873E-02
0.0954	160	3.4022E-04	1.2263E-03	5.5797E-04	5.9758E-03
0.0511	324	3.4849E-04	1.0508E-03	1.3521E-04	3.0401E-04
0.0356	448	3.5855E-04	9.3826E-04	1.2515E-04	1.2414E-04

that the use of $h_{\mathcal{S}} = 0.0954$ can reach the same orders of accuracy in the domain as those by smaller $h_{\mathcal{S}} = h_\Omega = 0.0511$.

6.3 Simulations on other surfaces

We run further simulations under different source terms on two more complicated geometries. They are surrounded by a constant distance product (CPD) surface[2] and an orthocircle[3].

[2] $\sqrt{(x-1)^2+y^2+z^2}\sqrt{(x+1)^2+y^2+z^2}\sqrt{x^2+(y-1)^2+z^2}\sqrt{x^2+(y+1)^2+z^2} - 1.1 = 0$.

[3] $[(x^2+y^2-1)^2+z^2][(y^2+z^2-1)^2+x^2][(x^2+z^2-1)^2+y^2] - 0.075^2[1+3(x^2+y^2+z^2)] = 0$.

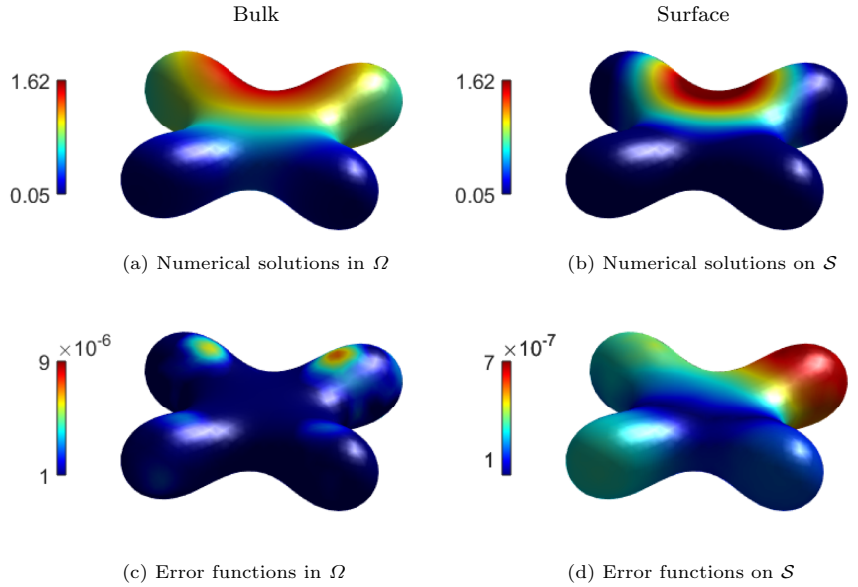

(a) Numerical solutions in Ω (b) Numerical solutions on $\mathcal{S}$

(c) Error functions in Ω (d) Error functions on $\mathcal{S}$

Fig. 9 Example 6.3.1: The numerical solutions (a-b) and error functions (c-d) in a CPD and on its boundary respectively, obtained by the boundary kernel of smoothness order $\mu_{\mathcal{S}} = 6$ and the bulk kernel of $\mu_B = 6.5$, using $(n_{X_\Omega}, n_{Z_\Omega}, n_{X_{\mathcal{S}}}, n_{Z_{\mathcal{S}}}) = (612, 566, 842, 614)$ with $h_X = 0.0147$ and $h_Z = 0.014$.

Example 6.3.1 ***With exact source terms.*** The first experiment is to apply the proposed oversampled approach in a domain surrounded by the CPD surface. The classical solutions u_B^* and $u_{\mathcal{S}}^*$ are selected as in (30). Figure 9(a)–(b) present our numerical results in Ω and on $\mathcal{S}$ respectively, and (c)–(d) are the corresponding error functions with detailed settings as follows: the boundary kernel of smoothness order $\mu_{\mathcal{S}} = 6$ and the bulk kernel of $\mu_B = 6.5$, and $(n_{X_\Omega}, n_{Z_\Omega}, n_{X_{\mathcal{S}}}, n_{Z_{\mathcal{S}}}) = (612, 566, 842, 614)$ with $h_X = 0.0147$ and $h_Z = 0.014$.. They show that the accuracy on the boundary is higher than that in the bulk at least one order of magnitude.

Example 6.3.2 ***Two different settings for source terms without exact solutions.*** Finally, we employ kernels of smoothness orders $\mu_{\mathcal{S}} = 6$ and $\mu_B = 6.5$. In two different cases of $(f_B, f_{\mathcal{S}}, g_{\mathcal{S}}) = (0, 1, 0)$ and $(f_B, f_{\mathcal{S}}, g_{\mathcal{S}}) = (1, 0, 0)$, our oversampled method solves the two problems inside and on the CPD and the orthocircle surfaces respectively. The numerical outcomes are plotted on two surfaces in (a) and (c) of Figures 10 and 11, as well as in both $\mathcal{S}$ and Ω in (b) and (d) of each figure for comparison. In Figures 10, solutions on boundaries are larger than those in bulk domains, but both of them follow the similar and symmetric distributions. On the contrary, results in Figures 11 tend to the reverse distributions, corresponding to the same domain in Figures 10. The values on the surfaces are smaller.

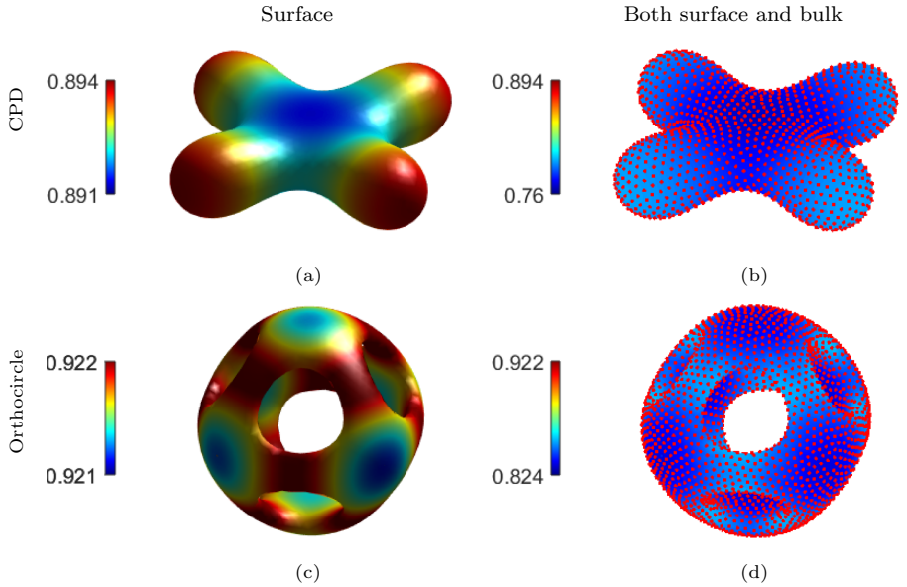

Fig. 10 Example 6.3.2: The numerical solutions by setting $(f_B, f_{\mathcal{S}}, g_{\mathcal{S}}) = (0, 1, 0)$ inside and on a CPD and an orthocircle respectively, obtained by using $\mu_{\mathcal{S}} = 6$ and $\mu_B = 6.5$ and oversampling $n_X > n_Z$.

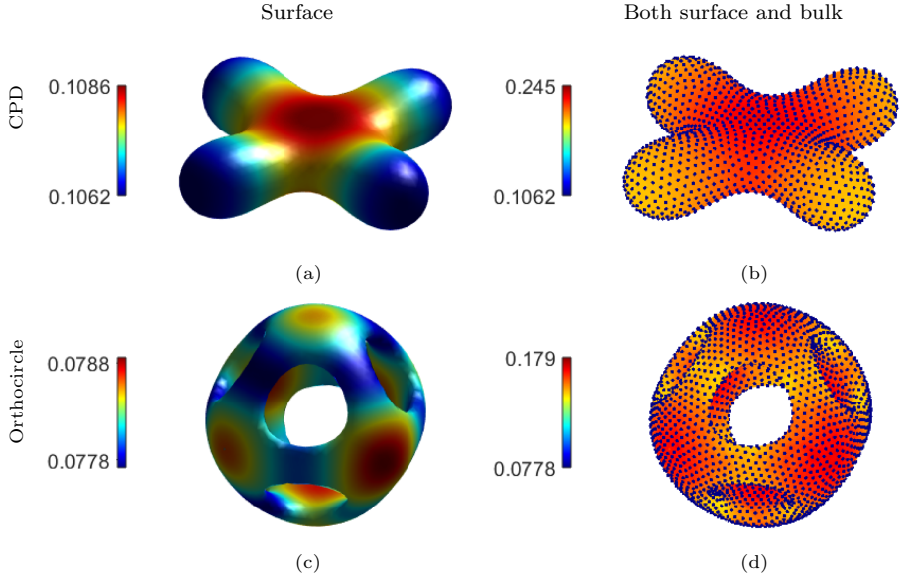

Fig. 11 Example 6.3.2: The numerical solutions by setting $(f_B, f_{\mathcal{S}}, g_{\mathcal{S}}) = (1, 0, 0)$ inside and on a CPD and an orthocircle respectively, obtained by using $\mu_{\mathcal{S}} = 6$ and $\mu_B = 6.5$ and oversampling $n_X > n_Z$.

7 Conclusion

This work was devoted to solve coupled bulk-surface PDE systems that model interactions in the bulk domains and on the surfaces, typically, connected through Robin boundary conditions. We modified convergence of least-squares RBF methods for solving elliptic PDEs with Dirichlet boundary conditions to a more general Robin type. Based on two kernel-based trial spaces for the two computational domains, we then decoupled the bulk-surface PDEs by assuming one of the solutions is available in order to study the connections between the bulk and surface kernels. A set of simulations was used to verify accuracy and convergence properties, as well as feasibility, of the proposed method on various domains and surfaces.

Overall, improvement in approximation power can be achieved in three ways. Using bulk kernels with higher orders than those of the surfaces is recommended. We also recommend using finer discretization on surfaces than in bulks, i.e., $h_{\mathcal{S}} < h_{\Omega}$. Oversampling in bulks is essential to convergence rate and sufficiently dense collocation points should be used.

References

1. Abels, H., Lam, K.F., Stinner, B.: Analysis of the diffuse domain approach for a bulk-surface coupled PDE system. SIAM J. Math. Anal. **47**(5), 3687–3725 (2015)
2. Burman, E., Hansbo, P., Larson, M.G., Zahedi, S.: Cut finite element methods for coupled bulk–surface problems. Numer. Math. **133**(2), 203–231 (2016)
3. Chechkin, A.V., Zaid, I.M., Lomholt, M.A., Sokolov, I.M., Metzler, R.: Bulk-mediated diffusion on a planar surface: Full solution. Phys. Rev. E **86**(4), 041101 (2012)
4. Chen, M., Ling, L.: Intrinsic meshless collocation methods for PDEs on manifolds. In review (2019)
5. Cheung, K.C., Ling, L.: A kernel-based embedding method and convergence analysis for surfaces PDEs. SIAM J. Sci. Comput. **40**(1), A266–A287 (2018)
6. Cheung, K.C., Ling, L., Schaback, R.: H^2-convergence of least-squares kernel collocation methods. SIAM J. Numer. Anal. **56**(1), 614–633 (2018)
7. Elliott, C.M., Ranner, T.: Finite element analysis for a coupled bulk–surface partial differential equation. IMA J. Numer. Anal. **33**(2), 377–402 (2013)
8. Fuselier, E., Wright, G.B.: Scattered data interpolant on embedded submanifolds with restricted positive definite kernels: Sobolev error estimates. SIAM J. Numer. Anal. **50**(3), 1753–1776 (2012). DOI 10.1137/110821846
9. Garate, I., Glazman, L.: Weak localization and antilocalization in topological insulator thin films with coherent bulk-surface coupling. Phys. Rev. B **86**(3), 035422 (2012)
10. Giesl, P., Wendland, H.: Meshless collocation: Error estimates with application to dynamical systems. SIAM J. Numer. Anal. **45**(4), 1723–1741 (2007)
11. Macdonald, C.B., Ruuth, S.J.: Level set equations on surfaces via the closest point method. J. Sci. Comput. **35**(2-3), 219–240 (2008). DOI 10.1007/s10915-008-9196-6
12. Macdonald, C.B., Ruuth, S.J.: The implicit closest point method for the numerical solution of partial differential equations on surfaces. SIAM J. Sci. Comput. **31**(6), 4330–4350 (2009). DOI 10.1137/080740003
13. März, T., Macdonald, C.B.: Calculus on surfaces with general closest point functions. SIAM J. Numer. Anal. **50**(6), 145–189 (2012). DOI 10.1137/120865537
14. Matérn, B.: Spatial variation, vol. 36. Springer Science & Business Media (2013)
15. Medvedev, E., Stuchebrukhov, A.: Proton diffusion along biological membranes. J Phys Condens Matter **23**(23), 234103 (2011)

16. Narcowich, F.J., Sun, X., Ward, J.D.: Approximation power of RBFs and their associated SBFs: A connection. Adv. Comput. Math. **27**(1), 107–124 (2007). DOI 10.1007/s10444-005-7506-1
17. Nisbet, D.R., Rodda, A.E., Finkelstein, D.I., Horne, M.K., Forsythe, J.S., Shen, W.: Surface and bulk characterisation of electrospun membranes: Problems and improvements. Colloids Surf., B **71**(1), 1–12 (2009)
18. Piret, C.: The orthogonal gradients method: A radial basis functions method for solving partial differential equations on arbitrary surfaces. J. Comput. Phys. **231**(14), 4662–4675 (2012). DOI 10.1016/j.jcp.2012.03.007
19. Ruuth, S.J., Merriman, B.: A simple embedding method for solving partial differential equations on surfaces. J. Comput. Phys. **227**(3), 1943–1961 (2008). DOI 10.1016/j.jcp.2007.10.009
20. Umezu, K.: L^p approach to mixed boundary value problems for second-order elliptic operators. Tokyo J. of Math. **17**(1), 101–123 (1994). DOI 10.3836/tjm/1270128189
21. Wendland, H.: Error estimates for interpolation by compactly supported radial basis functions of minimal degree. J. Approx. Theory **93**(2), 258–272 (1998). DOI 10.1006/jath.1997.3137
22. Wloka, J.: Partial Differential Equations. Cambridge University Press (1987). DOI 10.1017/cbo9781139171755